

Soft Matter

Accepted Manuscript



This is an *Accepted Manuscript*, which has been through the Royal Society of Chemistry peer review process and has been accepted for publication.

Accepted Manuscripts are published online shortly after acceptance, before technical editing, formatting and proof reading. Using this free service, authors can make their results available to the community, in citable form, before we publish the edited article. We will replace this *Accepted Manuscript* with the edited and formatted *Advance Article* as soon as it is available.

You can find more information about *Accepted Manuscripts* in the [Information for Authors](#).

Please note that technical editing may introduce minor changes to the text and/or graphics, which may alter content. The journal's standard [Terms & Conditions](#) and the [Ethical guidelines](#) still apply. In no event shall the Royal Society of Chemistry be held responsible for any errors or omissions in this *Accepted Manuscript* or any consequences arising from the use of any information it contains.

The Effect of Nanoparticle Location and Shape on Thermal Transitions Observed in Hydrated Layer-by-Layer Assemblies

Cite this: DOI: 10.1039/x0xx00000x

Received 00th January 2014,
Accepted 00th January 2014

DOI: 10.1039/x0xx00000x

www.rsc.org/softmatter

Joseph T. Puhr,^a Benjamin E. Swerdlow,^b Dariya K. Reid^c and Jodie L. Lutkenhaus^{a,c}

Nanoparticles can have a profound effect on thermal transitions observed in polymer nanocomposites. Many layer-by-layer (LbL) assemblies contain nanoparticles for added functionality, but the resulting effects of nanoparticles on an LbL film's thermal properties are not known. Previously, we have shown that a nanoparticle-free LbL film containing strong polyelectrolytes, poly(diallyldimethylammonium chloride)/poly(styrene sulfonate) (PDAC/PSS), exhibited a single reversible thermal transition much like a glass-melt transition. In the work presented here, nanoparticles of either spherical (SiO₂) or platelet (Laponite clay) shape are inserted at varying vertical locations throughout PDAC/PSS LbL films. Temperature-controlled quartz crystal microbalance (QCM-D) and modulated differential scanning calorimetry (MDSC) are applied, for which QCM-D proved to be more sensitive to the transition. All Laponite-containing films possess two thermal transitions. During growth, Laponite-containing films exhibit steady increases in dissipation, which is proposed to arise from mechanically decoupled regions separated by the Laponite nanoparticles. For SiO₂-containing films, three transitions are detectable only when the SiO₂ nanoparticles were placed in the middle of the film; no transitions are observed for SiO₂ placed at the bottom or top, perhaps because of a weakening of the transition. The lowest transition is close in value to that of neat PDAC/PSS LbL films, and was assigned to a "bulk" response. The higher transition(s) is attributed to polymer chains in an interfacial region near the nanoparticle. We propose that nanoparticles restrict segmental mobility, thus elevating the transition temperature in the interfacial region.

1. Introduction

Layer-by-layer (LbL) assembly, a process by which nanoscale films are made through the alternating adsorption of oppositely charged species, has found use in a host of applications ranging from optics to drug delivery.¹⁻¹⁰ Precise control of film growth and subsequent properties can be exercised through simple adjustment of parameters such as ionic strength, salt type, pH, molecular weight, solvent quality, temperature, and humidity.¹¹⁻²⁰

To date, much remains to be learned about the thermal behavior of LbL films. This issue becomes relevant considering that the viability of LbL films in certain applications depends on whether they are glassy or rubbery. In the past few years a number of thermal characterization techniques have been utilized to study the thermophysical properties of LbL films, including microdifferential scanning calorimetry (micro-DSC), swelling/shrinking of LbL capsules, NMR spectroscopy, and electrochemical impedance spectroscopy.²¹⁻²⁴

Recently, our group has demonstrated that thermal transitions in hydrated LbL films can be measured via quartz crystal microbalance with dissipation (QCM-D).^{25, 26} QCM-D differentiates itself from other potential thermoanalytical techniques by its capacity to observe changes in both hydrated film mass and viscoelasticity as a function of film depth using overtones. The greater sensitivity of these measurements has proven useful in detecting especially weak transitions. Using QCM-D, we have previously examined hydrated LbL films of both strong and weak polyelectrolyte systems, namely poly(diallyldimethylammonium chloride)/poly(styrene sulfonate) (PDAC/PSS) and poly(allylamine hydrochloride)/poly(acrylic acid) (PAH/PAA), respectively.^{25, 26} Both systems exhibit a second-order thermal transition, in which the film softens upon heating. In a forthcoming publication, we show that the transition exhibits both lower critical solution temperature (LCST) and glass transition-like character, in which extrinsically compensated functional groups

on the polyelectrolyte dehydrate upon heating, thus inducing a change in the polymer's segmental mobility.

Nanoparticles are known to influence a polymer's LCST, for which most studies focus on poly(*N*-isopropylacrylamide) (PNIPAM), a thermoreversible polymer with a sharp LCST.²⁷ For example, Schönhoff *et al.* studied the behavior of PNIPAM polymer and charged copolymer chains adsorbed to colloidal SiO₂, and found that in general the LCST both broadened and increased in temperature.²⁸ Additionally, Shan *et al.* observed two phase transitions for PNIPAM brushes adsorbed to Au nanoparticles via microcalorimetry.²⁹ This phenomenon was attributed to the existence of inner and outer PNIPAM zones surrounding the Au nanoparticle, with the former exhibiting a sharp, lower transition, and the latter showing a broad, higher transition. Similar results have been reported for the glass transition temperature of polymer nanocomposites.³⁰⁻³²

The PDAC/PSS LbL system is studied here as a model system because its properties and structure are very well described.^{15-17, 22, 23, 33-39} The system is strongly affected by the ionic strength of the assembly solution, which allows for the modulation of extrinsic to intrinsic charge compensation (*i.e.*, polyelectrolyte/counter-ion to polyelectrolyte/polyelectrolyte ion-pairing, respectively). Assembled with no added salt, the LbL film is dominated by intrinsic charge compensation, is highly cross-linked via ion-pairs, and does not exhibit any discernible thermal transition. As the ionic strength of the assembly solution increases, extrinsic charge compensation increases, the ion-pair cross-link density decreases, and the aforementioned thermal transition appears. A similar relationship between ionic strength (salt doping) and transition temperature has also been reported for PDAC/PSS complexes.⁴⁰

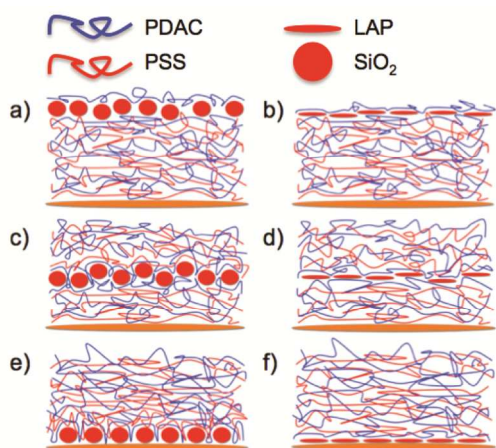


Figure 1. The various film configurations studied in this work. Panels a), c), and e) correspond to films incorporating SiO₂ nanoparticles, while panels b), d), and f) correspond to films incorporating Laponite (LAP) nanoplatelets.

Many LbL assemblies contain nanoparticles for added functionality, but their resulting effect on the film's thermal properties is not known. Here, we apply both QCM-D and modulated DSC (MDSC) to investigate the thermal properties of hydrated PDAC/PSS LbL films into which layers of negatively charged SiO₂ and Laponite RD (LAP) nanoparticles have been inserted (Figure 1). The ionic strength of the assembly solutions is fixed at 0.5 M NaCl, a condition upon which the neat LbL film is known to exhibit a thermal transition and to bear both intrinsically and extrinsically

compensated sites. Of particular interest are the effects that both nanoparticle shape (spherical vs. platelet) and location (near film-substrate interface vs. within the bulk vs. near the film's free surface) have on the previously measured thermal transitions in PDAC/PSS LbL films. This information allows us to understand how nanoparticles interact with LbL assemblies, whether the structure of these assemblies changes, and how thermal properties are affected.

2. Materials and Methods

2.1 Materials

Poly(diallyldimethylammonium chloride) (PDAC, $M_w = 350,000 \text{ g mol}^{-1}$) and poly(styrene sulfonate sodium salt) (PSS, $M_w = 500,000 \text{ g mol}^{-1}$) were purchased from Sigma Aldrich and Scientific Polymer Products, respectively. Poly(ethyleneimine) (PEI, $M_w = 25,000 \text{ g mol}^{-1}$) was purchased from Polysciences, Inc. Laponite RD (LAP, diameter of about 25 nm, thickness of 1 nm) was purchased from Southern Clay, while Ludox TM-40 (40 wt % SiO₂ suspension in water, average particle size of 22 nm, and specific surface area of $140 \text{ m}^2 \text{ g}^{-1}$) was purchased from Sigma-Aldrich. Teflon® and quartz crystal substrates were purchased from McMaster Carr and Q-Sense, respectively.

2.2 Preparation of Freestanding LbL Assemblies

PDAC and PSS solutions were made from their respective homopolymers and 18.2 MΩ cm (Milli-Q) water at a concentration of 1 mg mL^{-1} . The concentrations of the SiO₂ and LAP nanoparticle suspensions were both adjusted to 0.03 wt %. LbL assemblies were constructed using an automated slide stainer (HMS series, Carl Zeiss, Inc.). Teflon® substrates used to fabricate free-standing LbL assemblies were cleaned using sonication for 15 min in ethanol, followed by 15 min sonication in deionized water. Teflon® substrates were dipped in PDAC solution for 15 min, followed by three separate rinses with Milli-Q water for 2, 1, and 1 min, respectively. The substrates were then dipped in PSS solution for 15 min, followed by another series of water rinses as before. Whenever the inclusion of a nanoparticle (NP) layer was required, the NP solution would take the position of PSS in the assembly process. The ionic strength of assembly for all baths was 0.5 M NaCl in order for comparisons to be made with a previous study by our group.²⁵ The freestanding films that were assembled can be generalized using the following notation for which the subscript denotes the number of layer pairs: (PDAC/PSS)₁₄₉(PDAC/NP)₁, (PDAC/PSS)₇₄(PDAC/NP)₂(PDAC/PSS)₇₄, and (PDAC/NP)₁(PDAC/PSS)₁₄₉. These configurations were chosen so as to test the effect that NP location has on the film's thermal transition temperature (*i.e.* near the free surface, bulk, or the film-substrate interface, respectively). The LbL films were then dried in ambient air and stored in a desiccator until further use. The films were isolated from their Teflon® substrates just before MDSC experiments. For atomic force microscopy (AFM), samples PDAC/PSS LbL films were assembled on silicon with the penultimate layer being PDAC and the ultimate layer being either LAP or SiO₂ nanoparticles.

2.3 Preparation of LbL Assemblies Using QCM-D

All QCM-D experiments were performed using the Q-Sense E1 system at 25 °C. Gold-plated AT-cut quartz crystals (resonant frequency of 5 MHz) were first plasma treated for 10 min followed by a 10 min immersion in a water/NH₄OH/H₂O₂ (5:1:1 by volume) mixture at 70 °C, dried using nitrogen, and

then plasma treated as before. Prior to initializing the LbL film assembly process, 1 mg mL⁻¹ PEI solution (pH 4.5) was passed over the crystal at a rate 200 μL min⁻¹ for 15 min, followed by a 5 min rinse using Milli-Q water (pH 4.5). Dilute HCl and NaOH was used to adjust the pH. This initial layer was considered the zeroth layer and was used as a baseline for all QCM-D experiments. This baseline was allowed to equilibrate until changes of no more than ± 2 Hz and ± 0.5 dissipation units were observed. Then, 0.1 mg mL⁻¹ PSS solution was passed over the crystal at a flow rate of 200 μL min⁻¹ for 15 min, followed by a 5 min rinse using MilliQ water. Next, 0.1 mg mL⁻¹ PDAC solution was passed for 15 min, followed by rinsing as before. Whenever a nanoparticle layer was required, 0.0015 wt % suspensions of either SiO₂ or LAP were passed over the crystal for 15 min, followed by a 5 min rinse as previously described. With the exception of the PEI solution, all polymer solutions and nanoparticle suspensions used during the assembly process were at an ionic strength of 0.5 M NaCl. The assembled films can be generalized using the following notation: PEI(PSS/PDAC)₆(NP/PDAC)₁, PEI(PSS/PDAC)₃(NP/PDAC)₁(PSS/PDAC)₃, and PEI(NP/PDAC)₁(PSS/PDAC)₆. These configurations were chosen so as to test the effect that NP location has on the film's thermal transition temperature (*i.e.* near the free surface, bulk, or the film-substrate interface, respectively).

2.4 Thermal Analysis of LbL Assemblies Using QCM-D

Thermal analysis of hydrated LbL assemblies using QCM-D was achieved by means of a temperature program created with the QSoft Software (Q-Sense). Heating cycles were performed at a rate of 1 °C min⁻¹ over temperatures ranging from 30 to 70 °C. Cooling cycles were also performed; however, the transitions were very weak and un-reproducible and thus were not included in our analysis. Prior to beginning a typical experiment, the newly assembled film was allowed to sit under flow of a 0.5 M NaCl solution for 1 hour at 25 °C. Then a stable baseline was established by holding the film at the desired starting temperature for several minutes. This baseline was required to deviate no more than ± 2 Hz and ± 0.5 dissipation units before initiating the temperature ramping program. Throughout the entire experiment, a 0.5 M NaCl solution was continually passed through the cell at a flow rate of 200 μL min⁻¹. Due to the fact that both density and viscosity of water are functions of temperature, the submerged crystal response will bear its own unique response.⁴¹ Thus to properly isolate the response of the LbL film alone, the temperature-dependent response of the bare crystal was subtracted from the raw data. In order to generate this temperature correction, a collection of at least 5 bare crystal measurements was obtained. These measurements were averaged and a linear trend line was then fit to both the Δ*F* and Δ*D* data (Figures S1 and S2, Tables S1 and S2). Following this subtraction procedure, the resulting values were shifted vertically on the y-axis such that both Δ*F* and Δ*D* were zero at 30 °C. This resulted in the “corrected data” used for our analysis. Transitions were deemed “repeatable” if greater than 2/3 of samples exhibited the transition, the value of which did not vary significantly. Poor crystal quality or reusing crystals was identified as a major contributor to those samples not exhibiting a transition.

2.5 Modeling of QCM-D Data

The Sauerbrey equation,⁴² which relates change in frequency and the adsorbed mass, was found to inadequately describe the films analysed in this study, as was the standard

Voigt model.⁴³ The former is suitable for thin, rigid films, while the latter is suitable for soft, viscous films; both models a homogeneous film distribution. We found that the frequency-dependent extended Voigt model fit our data best, which allows for a frequency-dependant shear elastic modulus and viscosity,⁴⁴ ESI. The QTools modeling software (Q-Sense) took all overtones (*n* = 3-13) into consideration. Table S3 lists the parameters that were used in the modeling process.

2.6 Modulated Differential Scanning Calorimetry

Because the transition was weak, conventional DSC was found to be unreliable. Instead, MDSC (TA Instruments DSC Q200) was performed on film samples in heat-cool-heat cycles. LbL films were hydrated with 12 wt % of 0.5 M NaCl solution, and the total MDSC sample mass ranged between 5 and 15 mg, depending on sample availability. Tzero hermetic pans and lids were used (TA Instruments). Hydrated films were ramped from 0 to 115 °C at a rate of 2 °C min⁻¹ with amplitude of 1.272 °C for a period of 60 s. All transitions reported were taken from the second heating cycle.

3. Results and Discussion

We performed QCM-D experiments on PDAC/PSS LbL films assembled from solutions of 0.5 M NaCl where nanoparticles of either spherical or platelet morphology were inserted at varying intervals (Figure 1). Our motivation was to determine how both nanoparticle morphology and relative location within the film influences the thermal transition. Previously, we have observed that neat PDAC/PSS LbL films assembled from solutions of 0.5 M NaCl possessed a transition temperature of 53 ± 1 °C.²⁵

Figure 2 depicts both the raw and fitted (solid black line) assembly data for the build-up of various LbL assemblies monitored via QCM-D. As the films were assembled within the cell, changes in frequency (Δ*F*) and dissipation (Δ*D*) were simultaneously recorded. A decrease in Δ*F* indicates an increase in hydrated film mass, while an increase in Δ*D* indicates a decrease in shear viscosity and elastic modulus. The extended Voigt model was applied to the assembly data, and the resulting fits enabled the determination of thickness for the various film configurations. It was observed that the fit began to slightly deviate from the experimental data following the addition of the nanoparticle layer (Figure S3).

Previously shown,³ nanoparticle-free PDAC/PSS LbL films exhibit step-wise decreases in Δ*F*, associated with nonlinear or “exponential” growth, and Δ*D* increases upon adsorption of the first layer, followed by an oscillation over a constant value. Here, the insertion of either spherical SiO₂ or platelet LAP nanoparticles during assembly resulted in markedly different assembly behaviours from that of the neat film. Panels (a), (c), and (e) of Figure 2 correspond to both the 3rd and 13th overtone measurements for PDAC/PSS LbL films that incorporate SiO₂. For all film configurations, the SiO₂ adsorption step leads to large decreases in Δ*F* as well as large increases in Δ*D* (increased hydrated mass and decreased viscosity/modulus, respectively). Interestingly, when SiO₂ is added either within the first or middle layer pairs, dissipation decreases for the remainder of the assembly experiment. We speculate that this behavior is attributed to the nanoparticles slowly embedding themselves in the film during assembly, thereby leading to film densification. SiO₂ embedment into PDAC has also been observed by Xu *et al.*⁴⁵

Panels (b), (d), and (f) of Figure 2 correspond to both the 3rd and 13th overtone measurements for PDAC/PSS LbL films that incorporate LAP. Upon adsorption of the LAP layer, very little change in frequency and dissipation are observed. After the LAP adsorption step, subsequent layer adsorption results in a continually increasing trend in dissipation for the remainder of the assembly experiment. A potential explanation for this

occurrence is that the rigid LAP layer creates two mutually exclusive regions within the film. Thus as the quartz crystal oscillates, the portion of the film below the LAP layer will move out of phase to that of the remaining film above. A diagram proposing this phenomenon is shown in Figure 3.

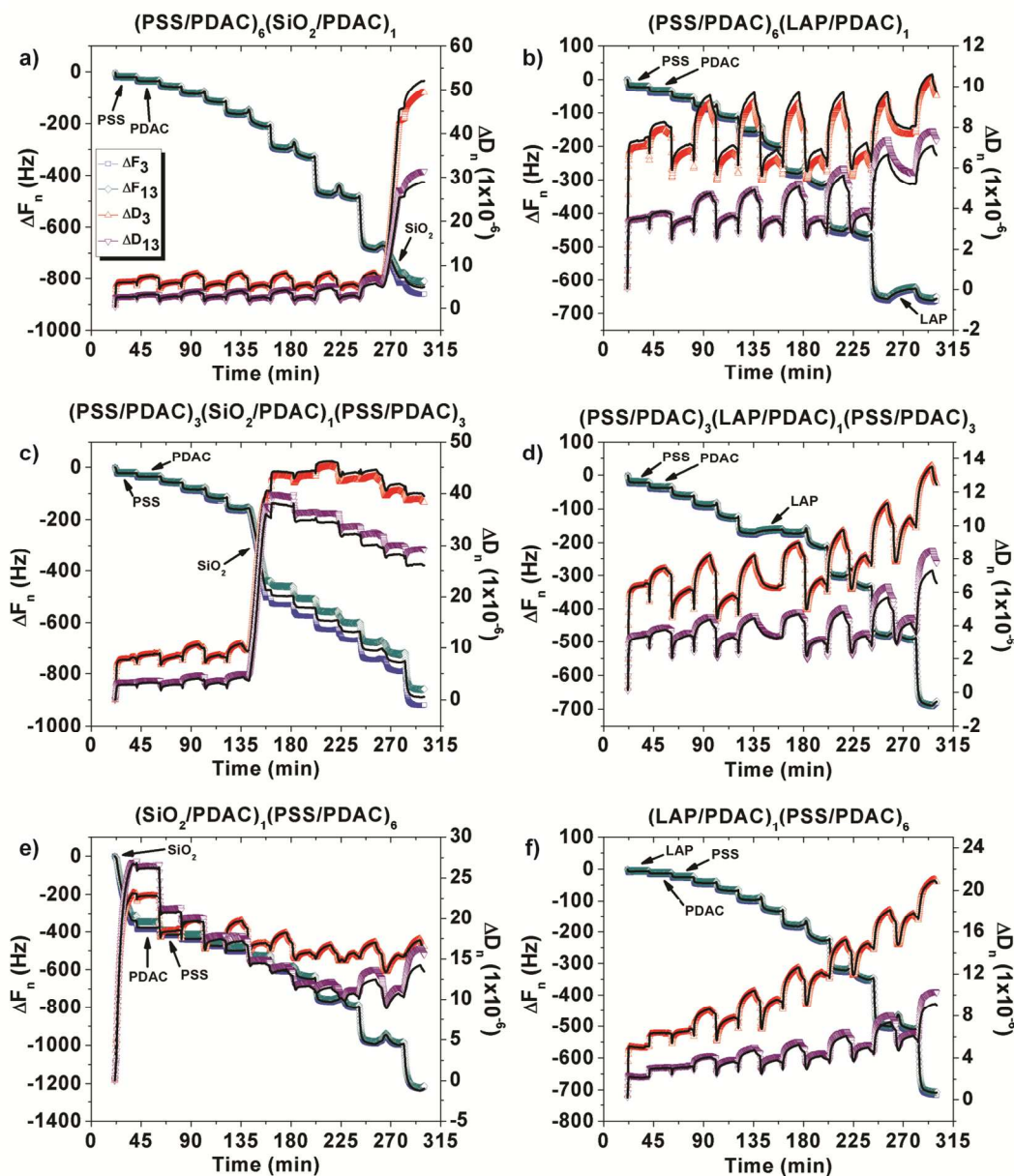


Figure 2. Raw ($\Delta F_3 =$ blue, $\Delta F_{13} =$ turquoise, $\Delta D_3 =$ red, and $\Delta D_{13} =$ purple) and fitted (black lines) data for the 3rd and 13th overtones of PDAC/PSS films incorporating SiO₂ either LAP. Panels a and b correspond to films where the nanoparticles were added within the last layer pair, panels c and d correspond to films where the nanoparticles were added in the center, and panel e and f corresponds to films where the nanoparticles were added within the first layer pair. The legend in panel (a) applies to all panels.

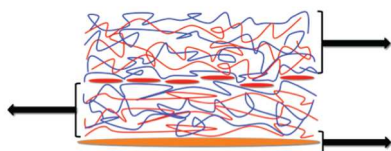


Figure 3. Illustration of possible viscoelastic behavior in hydrated LAP-containing PDAC/PSS films. The LAP nanoplatelet layer in the center perhaps acts as a rigid filler in which the LbL film above and below the layer move in a decoupled fashion.

Figure 4 illustrates the film thicknesses that were obtained from an extended Voigt model applied to the data shown in Figure 3. Figure 4a corresponds to various film arrangements that incorporated SiO_2 nanoparticles; the thickest film resulted when SiO_2 was added in the first layer pair. When SiO_2 was adsorbed in the middle of the film, exponential growth was interrupted. Figure 4b corresponds to the different film configurations that included LAP; the three films incorporating LAP all conclude with roughly the same thickness- a thickness that is significantly smaller than the neat (PDAC/PSS)₇ LbL film. This reduced thickness is attributed to the interruption of exponential growth and to the low thickness of the LAP nanoplatelets, which are only about 1 nm in thickness and have been shown to adsorb parallel to the film surface.⁴⁶

To view the adsorbed particles, atomic force microscopy was conducted on a PDAC/PSS LbL film in which the top-most layer was last exposed to either LAP or SiO_2 nanoparticles. The images show good coverage of the surface for both nanoparticle types and demonstrate particle sizes commensurate with that reported by the manufacturer. This good coverage is consistent with the step-wise increases in thickness observed for SiO_2 adsorption in Figure 4a. The LAP nanoparticles appear to lay flat against the LbL surface, which is consistent with the negligible change in thickness upon LAP adsorption in Figure 4b.

Following assembly, the films were allowed to equilibrate in the QCM-D cell under flow of 0.5 M NaCl in water, and then heated from 30 to 70 °C at 1 °C min⁻¹. As mentioned earlier, both density and viscosity of water are functions of temperature, and, as a result, they will influence the submerged crystal's response.⁴¹ Thus in order to properly isolate the response of the LbL film, the temperature-dependent response of the bare crystal must be subtracted from the raw data (Figures S1 and S2). This subtraction procedure generates the "corrected data" shown in both Figures 6 and 7.

A very useful feature of QCM-D, especially considering the aims of this study, is its capability to determine ΔF and ΔD values averaged over various depths through the film by means of overtones. Each particular overtone has an associated penetration depth dependent upon the decay length of the evanescent wave in contact with the film and bulk fluid. This depth decreases with increasing overtone number, meaning that lower overtones are more ideally suited for probing the film-substrate interface.^{47, 48} For example in pure water at 20 °C, this penetration depth is roughly 145 nm for the 3rd overtone, but just 50 nm for the 13th overtone. We therefore were able to apply this feature in order to better determine the role that nanoparticle layer location played in influencing the thermal transitions observed for PDAC/PSS films.

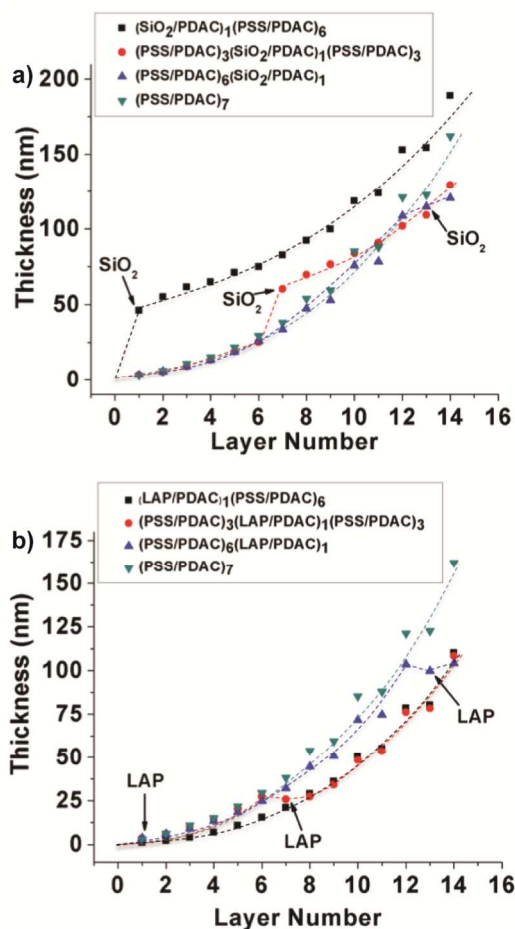


Figure 4. Film thicknesses determined by means of the extended Voigt model for PDAC/PSS films incorporating nanoparticles of either spherical or platelet morphologies. Panel a) depicts SiO_2 -containing films while panel b) depicts LAP-containing films. Note: (NP/PDAC)₁(PSS/PDAC)₆ = black, (PSS/PDAC)₃(NP/PDAC)₁(PSS/PDAC)₃ = red, (PSS/PDAC)₆(NP/PDAC)₁ = blue, and (PSS/PDAC)₇ = turquoise. Dotted lines have been included to "guide" the eye.

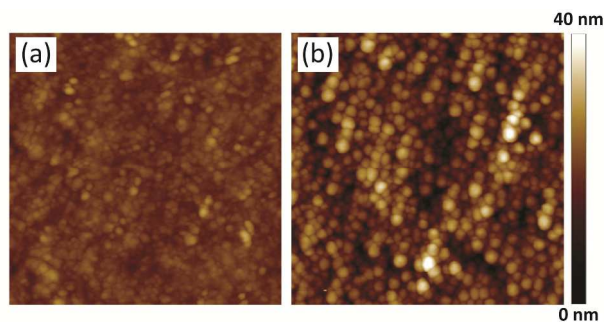


Figure 5. AFM images PDAC/PSS LbL assemblies in which (a) LAP or (b) SiO_2 nanoparticles are the top-most layer. Both images are 1x1 μm^2 . The z-scale at right applies to both images.

In general, for films that incorporate SiO_2 nanoparticles (Figure 6), ΔF values increased slightly with increasing temperature, corresponding to a small decrease in the film's hydrated mass. Thermal transitions were repeatedly observed

only in the case of the $(\text{PSS}/\text{PDAC})_3(\text{SiO}_2/\text{PDAC})_1(\text{PSS}/\text{PDAC})_3$ film configuration, for which ΔF exhibited abrupt decreases in ΔF at 56, 61, and 67 °C, corresponding to a sudden influx of water into the film. Concurrently, there were also increases in ΔD values at these same temperatures, implying a softening of the film. As shown in our prior work,²⁴ these abrupt changes in ΔF are hallmarks of a thermal transition. The low-temperature transition (56 °C) is consistent with our prior report for neat PDAC/PSS LbL films, but the high-temperature transitions are new features, which we attribute to the presence of the SiO_2 nanoparticles. It has been shown that nanoparticles can reduce polymer dynamics in the polymer-nanoparticle interphase, leading to elevated glass transitions and LCSTs.²⁸⁻³⁰ Elsewhere, it has been proposed that these stepwise changes could arise from the surpassing of various weak interaction energy barriers necessary for rearrangement to occur within the nanoparticle layer.⁴⁹ It is curious that the transition was not reproducibly detectable for films possessing SiO_2 nanoparticles in bottom or top layers. The significance of this is not yet clear, but is perhaps attributed to a weakening of the transition such that it was beyond the limits of our detection.

The relationship between overtones and the strength (stepwise increase in ΔF and ΔD) of the transition was opposite of that observed for neat PDAC/PSS LbL films.²⁵ For the neat film, a larger response from the 13th overtone (near the film-substrate interface) at the thermal transition as compared to the 3rd overtone (which penetrates farther into the film), indicating that structural rearrangement was more prominent near the crystal. This is consistent with Schlenoff's report that the region near the substrate possesses more extrinsic compensation, thus yielding a stronger transition.³⁹ As seen in Figure 6c and 6d, the opposite holds true for the $(\text{PSS}/\text{PDAC})_3(\text{SiO}_2/\text{PDAC})_1(\text{PSS}/\text{PDAC})_3$ LbL configuration. This behaviour may be attributed to a weakening of the transition for the region between the nanoparticles and the substrate, for which there exists two rigid boundaries. This implies that the majority of the polymer chains participating in the transition are near or above the SiO_2 layer.

In contrast, markedly different behavior was observed for films that incorporated LAP nanoplatelets (Figure 7). Unlike the films incorporating SiO_2 , there were repeatable thermal transitions observed for all LAP film configurations. For the case of the $(\text{PSS}/\text{PDAC})_6(\text{LAP}/\text{PDAC})_1$ LbL film (panels a and b of Figure 7), two abrupt drops were observed in ΔF , one at roughly 55 °C and the other at about 65 °C. Concurrently, there were also slight jumps in ΔD at the same temperatures. $(\text{PSS}/\text{PDAC})_3(\text{LAP}/\text{PDAC})_1(\text{PSS}/\text{PDAC})_3$ and $(\text{LAP}/\text{PDAC})_1(\text{PSS}/\text{PDAC})_6$ LbL films behaved similarly, having transitions at 57/68 °C and at 55/65 °C, respectively. As was the case with SiO_2 films, the transitions observed for LAP films were more prominent for the 3rd overtone.

Modulated DSC (MDSC) was used to corroborate QCM-D findings. MDSC differs from conventional DSC in that rather than just a linear temperature ramp, both superimposed sinusoidal and linear temperature profiles are utilized. Therefore it becomes possible to separate overlapping thermal phenomena. The total heat flow measured via MDSC (related to the heat flow from a conventional DSC) is the sum of both the "reversing heat flow" and the "non-reversing heat flow," which contain information regarding the thermal response occurring at time scales below and above the modulation period, respectively. MDSC is especially useful for weak transitions, although we have previously shown that QCM-D is far more sensitive for observing thermal transitions in hydrated PDAC/PSS LbL assemblies.²⁵

MDSC scans were performed for bulk nanoparticle-containing PDAC/PSS films that were analogous in configuration to those used in QCM-D experiments (Figure S4). There were no discernable thermal transitions observed for hydrated films incorporating SiO_2 . Considering that the transition is known to occur for neat films and that QCM-D of SiO_2 -containing films (Figure 6) yielded a transition for only one of the three configurations, it is possible that SiO_2 nanoparticles weaken the transition such that it is not detectable.

In the case of LAP-containing hydrated films however, transitions were observed in roughly half of all samples (Table 2). Each configuration exhibited a single weak, broad transition that fell within error of the neat PDAC/PSS LbL film and the low-temperature transitions found herein using QCM-D. Still, the error was quite large, as is typical of these films for MDSC, thus preventing further conclusions to be drawn.

We next compare the nature of the thermal transitions observed using QCM-D as it relates to nanoparticle location and shape for the assembled LbL films, Table 1. There was little difference observed between the transition values for the two investigated morphologies. The main distinction was that normally two thermal transitions were observed for LAP-containing films, while three such transitions were noted for only a single SiO_2 -containing film. For all films exhibiting transitions, the low-temperature thermal transition was in the vicinity of, but slightly elevated relative to, that of neat PDAC/PSS LbL films assembled at an ionic strength of 0.5 M NaCl (53 ± 1 °C). Therefore, the low-temperature transition temperature likely corresponds to the neat PDAC/PSS layers, while any additional higher transitions correspond to polymer chains in the immediate vicinity of the nanoparticles for which higher temperatures are required for their subsequent relaxation. Schlenoff has discussed the transition in terms of "sticky reputation" and dynamic bond breaking.⁴⁰ Under this context, the higher transitions could correspond to the relaxation of polymers chains interacting with "stickier" nanoparticles, requiring higher temperatures to gain segmental mobility.

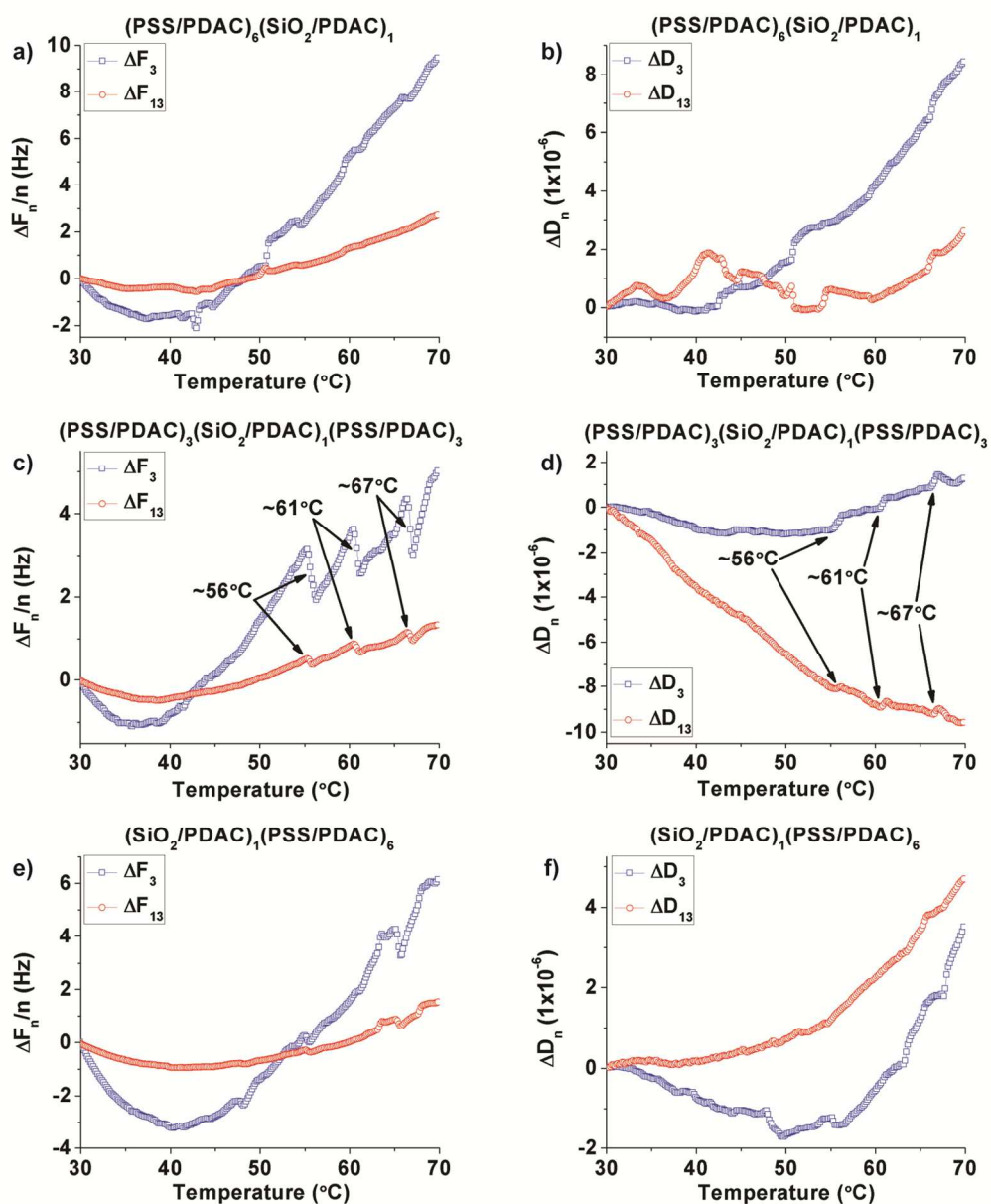


Figure 6. Corrected ΔF and ΔD for the 3rd and 13th overtones of PDAC/PSS LbL films incorporating SiO_2 . Panels a) and b) correspond to films where SiO_2 was added within the last layer pair, panels c) and d) correspond to films where SiO_2 was added in the central layer pair, and panels e) and f) correspond to films where SiO_2 was added within the first layer pair. The thermal transitions are indicated with arrows.

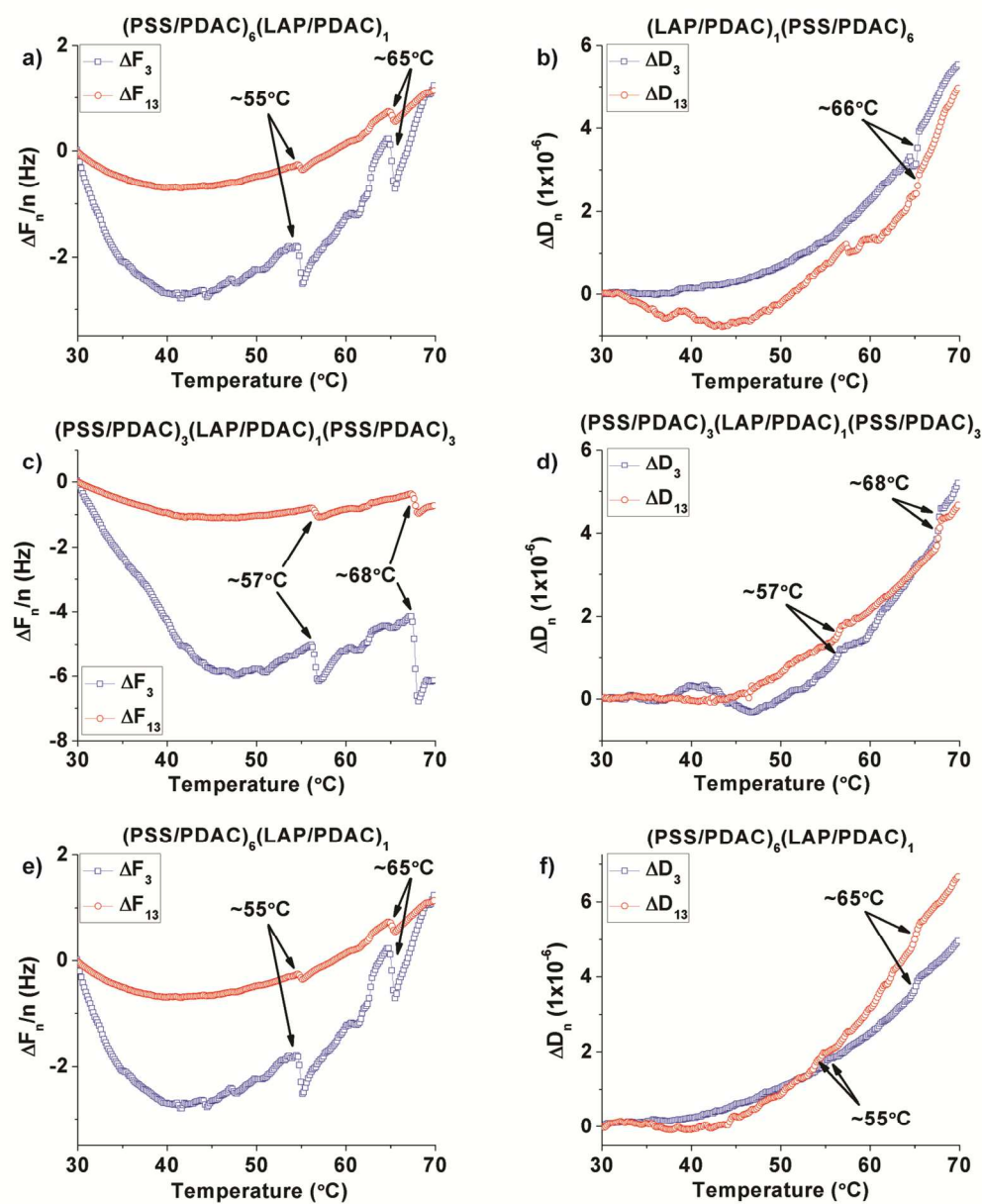


Figure 7. Corrected ΔF and ΔD for the 3rd and 13th overtones for PDAC/PSS LbL films incorporating LAP. Panels a) and b) correspond to films where LAP was added within the last layer pair, panels c) and d) correspond to films where LAP was added in the central layer pair, and panels e) and f) correspond to films where LAP was added within the first layer pair. The thermal transitions are indicated with arrows.

Table 1. Thermal Transition Values Obtained via QCM-D for Hydrated PDAC/PSS LbL Films Incorporating Nanoparticles.

Film Configuration	Averaged Thermal Transition Temperature
(PDAC/PSS) ₆ (PDAC/LAP) ₁	57 ± 3
(PDAC/PSS) ₃ (PDAC/LAP) ₁ (PDAC/PSS) ₃	64 ± 1
(PDAC/LAP) ₁ (PDAC/PSS) ₆	58 ± 2
(PDAC/PSS) ₆ (PDAC/SiO ₂) ₁	66 ± 2
(PDAC/PSS) ₃ (PDAC/SiO ₂) ₁ (PDAC/PSS) ₃	62 ± 2
(PDAC/SiO ₂) ₁ (PDAC/PSS) ₆	None
	56 ± 2
	62 ± 2
	68 ± 1
	None

Table 2. Thermal Transition Values Obtained via MDSC for Hydrated PDAC/PSS LbL Films Incorporating LAP Nanoplatelets.

LAP Film Configuration	Averaged Thermal Transition Temperature (°C)
(PDAC/PSS) ₁₄₉ (PDAC/LAP) ₁	46 ± 6
(PDAC/PSS) ₇₄ (PDAC/LAP) ₂ (PDAC/PSS) ₇₄	56 ± 9
(PDAC/LAP) ₁ (PDAC/PSS) ₁₄₉	50 ± 11

Conclusions

The growth and thermal properties of hydrated PDAC/PSS LbL films incorporating both spherical (SiO₂) and platelet (LAP) nanoparticles at varying locations were investigated.

Films grew similarly to exponentially growing PDAC/PSS LbL films with the exception that the nanoparticles appeared to “reset” or “restart” exponential growth. Interestingly, LAP-containing films exhibited anomalous increases in dissipation following LAP adsorption, which we attribute to regions mechanically isolated by the LAP platelets.

QCM-D proved more sensitive in detecting the transition relative to MDSC. Reproducible thermal transitions occurred in all LAP-containing films (LAP placed in the bottom, middle, or top layers). For SiO₂-containing films, the transitions were only detectable when the SiO₂ nanoparticles were placed in the middle of the film. Whereas the neat PDAC/PSS LbL film possessed only one transition, the LAP-containing films possessed two and the SiO₂-containing film possessed three. The lowest transition was close in value to that of neat PDAC/PSS LbL films, and was assigned to a “bulk” response. The higher transition(s) was attributed to polymer chains in an interfacial region near the nanoparticle. We proposed that the nanoparticle restricted segmental mobility, thus elevating the transition temperature.

The nature of the thermal transitions in hydrated LbL assemblies is still a subject of intense study. Future work will focus on thermal analysis of PDAC/PSS complexes and accompanying simulations.

Acknowledgements

This work was supported in part by the National Science Foundation Grant No. 1049706. We thank Dr. Archana Jaiswal from Q-Sense for assistance with QCM-D analysis.

Notes and references

^aDepartment of Materials Science & Engineering, Texas A&M University, College Station, TX 77843.

^bDepartment of Materials Science & Engineering, University of Florida, Gainesville, FL 32611.

^cArtie McFerrin Department of Chemical Engineering, Texas A&M University, College Station, TX 77843.

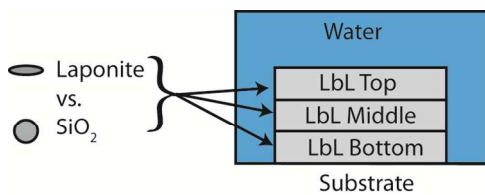
Electronic Supplementary Information (ESI) available: [details of any supplementary information available should be included here]. See DOI: 10.1039/b000000x/

1. R. K. Iler, *Journal of Colloid and Interface Science*, 1966, **21**, 569-594.
2. G. Decher, *Science*, 1997, **277**, 1232-1237.

3. Y. Wang, A. S. Angelatos and F. Caruso, *Chem. Mat.*, 2008, **20**, 848-858.
4. M. Delcea, H. Mohwald and A. G. Skirtach, *Advanced Drug Delivery Reviews*, 2011, **63**, 730-747.
5. J. L. Lutkenhaus and P. T. Hammond, *Soft Matter*, 2007, **3**, 804-816.
6. L. Zhai, M. C. Berg, F. C. Cebeci, Y. Kim, J. M. Milwid, M. F. Rubner and R. E. Cohen, *Nano Lett.*, 2006, **6**, 1213-1217.
7. J. Hiller, J. D. Mendelsohn and M. F. Rubner, *Nat. Mater.*, 2002, **1**, 59-63.
8. G. Decher, B. Lehr, K. Lowack, Y. Lvov and J. Schmitt, *New Nanocomposite Films For Biosensors - Layer-by-Layer Adsorbed Films of Polyelectrolytes, Proteins, or DNA*, Frankfurt, Germany, 1993.
9. K. Ariga, J. P. Hill, M. V. Lee, A. Vinu, R. Charvet and S. Acharya, *Sci. Technol. Adv. Mater.*, 2008, **9**, 96.
10. G. B. Sukhorukov and H. Mohwald, *Trends Biotechnol.*, 2007, **25**, 93-98.
11. R. v. Klitzing, *Physical Chemistry Chemical Physics*, 2006, **8**, 5012-5033.
12. S. T. Dubas and J. B. Schlenoff, *Macromolecules*, 1999, **32**, 8153-8160.
13. J. Choi and M. F. Rubner, *Macromolecules*, 2005, **38**, 116-124.
14. S. Shiratori and M. F. Rubner, *Macromolecules*, 2000, **33**, 4213-4219.
15. E. Guzman, H. Ritacco, J. E. F. Rubio, R. G. Rubio and F. Ortega, *Soft Matter*, 2009, **5**, 2130-2142.
16. M. Salomaki, I. A. Vinokurov and J. Kankare, *Langmuir*, 2005, **21**, 11232-11240.
17. R. A. Ghostine and J. B. Schlenoff, *Langmuir*, 2011, **27**, 8241-8247.
18. K. Buscher, K. Graf, H. Ahrens and C. A. Helm, *Langmuir*, 2002, **18**, 3585-3591.
19. P. Nesder, M. Passvogel and C. A. Helm, *Macromolecules*, 2013, **46**, 5622-5629.
20. K. E. Secrist and A. J. Nolte, *Macromolecules*, 2011, **44**, 2859-2865.
21. B. Fortier-McGill and L. Reven, *Macromolecules*, 2008, **42**, 247-254.
22. K. Köhler, H. Möhwald and G. B. Sukhorukov, *The Journal of Physical Chemistry B*, 2006, **110**, 24002-24010.
23. K. Köhler, D. G. Shchukin, H. Möhwald and G. B. Sukhorukov, *The Journal of Physical Chemistry B*, 2005, **109**, 18250-18259.
24. C. Sung, K. Hearn and J. L. Lutkenhaus, *Accepted to Soft Matter*, 2014.
25. A. Vidyasagar, C. Sung, R. Gamble and J. L. Lutkenhaus, *ACS Nano*, 2012, **6**, 6174-6184.
26. A. Vidyasagar, C. Sung, K. Losensky and J. L. Lutkenhaus, *Macromolecules*, 2012, **45**, 9169-9176.
27. Y. J. Zhang, S. Furry, D. E. Bergbreiter and P. S. Cremer, *Journal of the American Chemical Society*, 2005, **127**, 14505-14510.
28. M. Schonhoff, A. Larsson, P. B. Welzel and D. Kuckling, *Journal of Physical Chemistry B*, 2002, **106**, 7800-7808.
29. J. Shan, J. Chen, M. Nuopponen and H. Tenhu, *Langmuir*, 2004, **20**, 4671-4676.
30. H. Oh and P. F. Green, *Nat. Mater.*, 2009, **8**, 139-143.
31. G. Tsagaropoulos and A. Eisenberg, *Macromolecules*, 1995, **28**, 6067-6077.
32. G. Tsagaropoulos and A. Eisenberg, *Macromolecules*, 1995, **28**, 396-398.
33. C. Gao, S. Leporatti, S. Moya, E. Donath and H. Möhwald, *Langmuir*, 2001, **17**, 3491-3495.

34. J. J. Iturri Ramos, S. Stahl, R. P. Richter and S. E. Moya, *Macromolecules*, 2010, **43**, 9063-9070.
35. R. Mueller, K. Köhler, R. Weinkamer, G. Sukhorukov and A. Fery, *Macromolecules*, 2005, **38**, 9766-9771.
36. T. Farhat, G. Yassin, S. T. Dubas and J. B. Schlenoff, *Langmuir*, 1999, **15**, 6621-6623.
37. J. B. Schlenoff, H. Ly and M. Li, *Journal of the American Chemical Society*, 1998, **120**, 7626-7634.
38. J. B. Schlenoff and S. T. Dubas, *Macromolecules*, 2001, **34**, 592-598.
39. R. A. Ghostine, M. Z. Markarian and J. B. Schlenoff, *Journal of the American Chemical Society*, 2013, **135**, 7636-7646.
40. R. F. Shamoun, H. H. Hariri, R. A. Ghostine and J. B. Schlenoff, *Macromolecules*, 2012, **45**, 9759-9767.
41. N. Ishida and S. Biggs, *Langmuir*, 2007, **23**, 11083-11088.
42. G. Sauerbrey, *Zeitschrift Fur Physik*, 1959, **155**, 206-222.
43. M. V. Voinova, M. Rodahl, M. Jonson and B. Kasemo, *Physica Scripta*, 1999, **59**, 391-396.
44. L. Sun, S. Svedhem and B. Åkerman, *Langmuir*, 2014.
45. D. Xu, C. Hodges, Y. L. Ding, S. Biggs, A. Brooker and D. York, *Langmuir*, 2010, **26**, 18105-18112.
46. E. R. Kleinfeld and G. S. Ferguson, *Science*, 1994, **265**, 370-373.
47. S. J. Martin, V. E. Granstaff and G. C. Frye, *Analytical Chemistry*, 1991, **63**, 2272-2281.
48. D. M. Zhu, J. J. Fang, B. Wu and X. B. Du, *Physical Review E*, 2008, **77**.
49. L. Zhang, G. Feng, Z. Zeravcic, T. Brugarolas, A. J. Liu and D. Lee, *Acs Nano*, 2013, **7**, 8043-8050.

Graphical Abstract.



How is T_r affected by nanoparticle shape and location?

When nanoparticles are inserted at different locations within a layer-by-layer (LbL) assembly, a second higher temperature thermal transition appears under select conditions.